

Robust Underwater Telemetry With Adaptive Turbo Multiband Equalization

Paul A. van Walree, *Member, IEEE*, and Geert Leus, *Senior Member, IEEE*

Abstract—In this paper, a multicarrier modulation scheme is presented for acoustic communication at low signal-to-noise ratios (SNRs). User bits are put through a rate 1/3 turbo encoder and interleaved with periodic training bits. A maximal-length sequence is prefixed for signal detection and equalizer convergence, and the resulting bit stream is simultaneously modulated onto multiple phase-shift keyed carriers. Since each subband carries the same symbol sequence, the baseband ensemble is amenable to multichannel equalization. An adaptive multiband equalizer is thus constructed for joint equalization and despreading of the frequency bands. Iterative equalization using soft information from the turbo decoder further enhances the receiver performance. A reduction in complexity is achieved by equipping the subbands with separate recursive least squares tap updates, yet guided by a common error signal. The proposed algorithms are tested on acoustic data from the Baltic Sea, using eight subbands of 460 Hz each, at an effective data rate of 75 b/s. Robust receiver operation is demonstrated at overall receive SNRs down to -12 dB in three different channels, which corresponds to an SNR per bit $E_b/N_0 = +5$ dB.

Index Terms—Covert communications, iterative equalization and decoding, multiband equalization, multicarrier spread spectrum (MCSS), underwater communications.

I. INTRODUCTION

THE research project “UUV Covert Acoustic Communications” explores methods for clandestine acoustic telemetry in littoral environments. A robust wireless datalink is to be established between a mother ship and an unmanned underwater vehicle (UUV) over ranges up to 50 km. Another objective is for the transmitted waveforms to ensure a low probability of detection by third parties. This implies a low data rate, which allows signals to be hidden in the ambient noise. This paper treats a candidate modulation tested during exploratory sea trials in 2007. A high level of message protection is realized through channel coding, repetition coding, and periodic training. The repetition coding is applied in the

frequency domain and is adaptively decoded at the receiver end by a multichannel equalizer.

Multichannel equalizers have been developed in the context of space-time signal processing [1], exploiting diverse signal signatures received on spatially separated antennas. The spatial dimension allows a level of signal enhancement and interference cancellation that cannot be achieved with single-receiver systems. Multichannel receivers have become an important part of high-rate acoustic communication systems, which need to function in unforgiving underwater environments characterized by a severe delay-Doppler spread. In this field, adaptive multichannel equalizers have a tradition since the early 1990s [2], [3]. However, applicability of a multichannel equalizer is not restricted to signals originating from different hydrophones, either directly [2], [3] or after beamforming [4], [5]. This paper applies multichannel equalization to a single hydrophone, jointly equalizing contiguous frequency bands which carry identical symbol streams. In the presence of multipath propagation, the frequency coherence is smaller than the subband separation, and the multicarrier equalizer will act as a maximal-ratio combiner that exploits the baseband frequency diversity. However, notice that a single-carrier signal transmitted in the same overall band has the same frequency diversity at its disposal. The difference is that the proposed multicarrier spread-spectrum (MCSS) scheme allows a process of joint equalization and despreading, as opposed to, for example, chip-level equalizers applied to direct-sequence spread-spectrum (DSSS) waveforms [6], [7].

With DSSS, routine despreading delivers a symbol estimate only after all constituent chips have been equalized. Hence, the chip decisions needed to update the filter coefficients cannot immediately profit from the spread-spectrum gain. Although strategies exist to alleviate this problem [6], it does not hinder the present approach at all as the multiband equalizer performs joint equalization and despreading. A relatively reliable symbol estimate is automatically obtained with each equalizer update. A potential disadvantage is a reduced channel tracking capability, because, unlike a chip-level equalizer, the multiband receiver has no possibilities for tap updates within a symbol. Existing MCSS work was presented in [8] and [9], whereas Kondo and Milstein [10] and Sourour and Nakagawa [11] combine the use of multiple frequency bands with DSSS to provide repetition coding in frequency and time. However, the described receivers lack the adaptive equalization and combining required for many underwater channels.

Repetition in time and frequency was also applied in [12] to achieve communication at low receive signal-to-noise ratios (SNRs). However, that paper considers orthogonal frequency-division multiplexing (OFDM), whereas this paper considers more traditional frequency-division multiplexing

Manuscript received June 26, 2008; revised April 15, 2009; accepted September 13, 2009. First published October 30, 2009; current version published November 25, 2009. This work was performed under the EUROPA MOU ERG No1, RTP 110.060 “UUV Covert Acoustic Communications.” The Dutch contribution to this project was supported by The Netherlands Ministry of Defence. The work of G. Leus was supported in part by NWO-STW under the VIDi program (DTC.6577).

Associate Editor: U. Mitra.

P. A. van Walree was with The Netherlands Organisation for Applied Scientific Research (TNO), 2509 JG The Hague, The Netherlands. He is now with the Norwegian Defence Research Establishment (FFI), NO-3191 Horten, Norway (e-mail: paul.vanwalree@ffi.no).

G. Leus is with the Faculty of Electrical Engineering, Mathematics and Computer Science, Delft University of Technology, 2628 CD Delft, The Netherlands (e-mail: g.j.t.leus@tudelft.nl).

Digital Object Identifier 10.1109/JOE.2009.2032997

(FDM) with far fewer carriers. Transmitter and receiver structures differ widely between these modulations. FDM can be considered as a compromise between a single-carrier system and OFDM.

For fast convergence and tracking, the multiband equalizer under consideration uses a recursive least squares (RLS) update algorithm. A well-known drawback of the RLS update is its computational complexity—a long delay spread in combination with multiple hydrophone channels often prohibits its use. The complexity of the present equalizer is reduced by a factor equal to the number of frequency bands. This is achieved by equipping all bands with separate RLS schemes, minimizing a common mean square error (MSE). If cross correlations between subbands are negligible, this construction performs as well as the optimal RLS scheme that combines all channels in a single vector. Note that the use of subbands was also employed in [13] to reduce the symbol rate and make the equalizers more manageable, but in that paper, the subbands carry independent bit streams and are equalized separately and independently. Joint multiband equalization, i.e., joint optimization of filter coefficients across bands, requires identical symbol sequences in all subbands.

The multiband tap coefficients are updated in an iterative fashion by an adaptive turbo approach that runs in different forward and backward passes. Adaptive turbo equalization differs from traditional turbo equalization [13]–[16] in the sense that channel estimation is bypassed. Existing adaptive turbo methods such as those in [13], [17], and [18] only use forward passes, which renders it difficult to track time-varying channels. Moreover, these methods use either soft decisions or unconditional hard symbol decisions in the update process, whereas the proposed multiband receiver uses conditional hard decisions. That is to say, the equalizers are updated through hard symbol decisions, but only if these symbols are reliable. Periodic training prevents the adaptive filter from derailing during the first equalization stage, when the turbo decoder output is not yet available. This paper is further organized in the following manner. Section II presents the modulation and the transmitter. Section III describes signal acquisition, the receiver architecture and parameter values, and discusses the differences with existing strategies. Sea trials are described in Section IV, which also shows and discusses results obtained on acoustic and synthetic data. Section V provides concluding remarks.

Notation: Uppercase boldfaced letters represent matrices, lowercase boldfaced letters represent column vectors; $(\cdot)^*$ denotes conjugate and $(\cdot)^T$ denotes nonconjugate transpose. $\Re(x)$ denotes the real part of x ; $E(\cdot)$ stands for the expectation; $\mathbf{0}_N$ denotes a vector with N zeros and $\mathbf{I}_{N \times N}$ denotes the $N \times N$ identity matrix.

II. TRANSMITTER

Fig. 1 and the left part of Fig. 2 illustrate the modulation scheme and the transmitter structure. The transmitted waveform uses $N = 8767$ binary phase-shift keyed symbols $z(n) \in \{-1, 1\}$, comprising $N_{\text{TT}} = 127$ (initial) training symbols for detection and equalizer convergence, $N_{\text{PT}} = 2880$ periodic

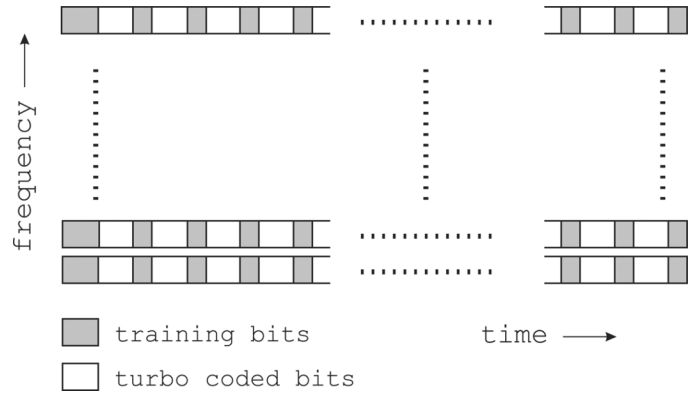


Fig. 1. Schematic depiction of the multicarrier modulation.

training bits, and $N_{\text{TC}} = 5760$ turbo coded bits. The initial training is a maximal-length m -sequence. A standard, rate $1/3$ parallel turbo encoder [19] is used with generator polynomial $(15, 13)$, which are the parity and feedback connections in decimal form. The interleaver internal to the turbo encoder has a length of 640 bits and encodes 637 information bits, as the three tail bits are reserved to terminate the first constituent encoder. Three code blocks are used. The coded bits and training bits are interleaved in 45 packets of 64 training bits and 128 code bits. The resulting symbol stream $\mathbf{z} = [z(1), \dots, z(N)]^T$ is simultaneously modulated onto $K = 8$ carriers to obtain the transmit waveform

$$s(t) = \sum_{k=1}^K \sum_{n=1}^N z(n)p(t - nT - k\Delta t) \exp[i\omega_k(t - k\Delta t)] \quad (1)$$

where ω_k gives the angular carrier frequency of the k th subband. T denotes the symbol period, with $T^{-1} = 345 \text{ s}^{-1}$ the symbol rate; $\Delta t = 1/6900 \text{ s}$ is a small timing offset which reduces the crest factor of the compound waveform from 17.1 to 10.7 dB. It causes an offset of less than half a symbol between the two outermost bands, and requires no compensation at a receiver equipped with an adaptive equalizer that spans a fair number of symbols. A raised-cosine spectrum [20, pp. 559–561] is adopted for the elementary pulse

$$p(t) = \text{sinc}\left(\frac{\pi t}{T}\right) \frac{\cos(\pi\beta t/T)}{1 - 4\beta^2 t^2/T^2} \quad (2)$$

using a rolloff factor $\beta = 1/3$. Its spectrum covers a total frequency band of $B = (1 + \beta)/T = 460 \text{ Hz}$. $K = 8$ of such bands are combined in a single waveform with a bandwidth of $KB = 3680 \text{ Hz}$. The carriers are connected to the overall center frequency ω_c by

$$\omega_k = \omega_c + 2\pi \left(k - \frac{K+1}{2}\right) B. \quad (3)$$

Guard bands are omitted as the smooth raised-cosine spectral rolloff provides sufficient protection against interband interference. The net data rate amounts to 3×637 information bits divided by a total signal duration of $NT = 25.4 \text{ s}$, which equals 75.2 b/s .

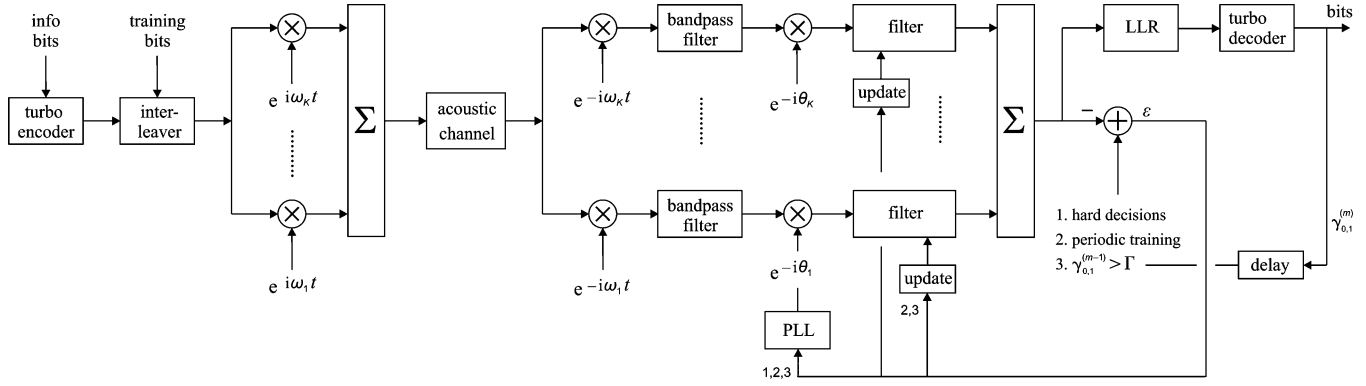


Fig. 2. Key elements of the transmitter and the receiver.

III. RECEIVER

The receiver operations consist of an acquisition stage; an adaptive-filter stage which implements joint equalization, de-spreading, and phase tracking; bit estimation; and application of a turbo decoder. Soft information from the turbo decoder is subsequently used to repeat the equalization stage with enhanced channel tracking capability.

A. Acquisition

The received data $\tilde{u}(t)$ are brought to complex baseband with respect to the overall center frequency

$$u(t) = \tilde{u}(t) \exp(-i\omega_c t) \quad (4)$$

and correlated with a bank of Doppler-shifted replicas of the detection part of the signal

$$r_v(t) = D_v \left(\sum_{k=1}^K \sum_{n=1}^{N_{\text{TR}}} z(n) p(t - nT - k\Delta t) \exp[i(\omega_k - \omega_c)(t - k\Delta t)] \right). \quad (5)$$

Since the signal is wideband, the Doppler shifts D_v are performed through resampling at a resampling factor of $1 + v/c$, where v is the relative transmitter/receiver velocity and c is the sound speed. Recorded data are fed to the correlator in root mean square (rms)-normalized blocks of several seconds. The peak correlator output is obtained across all Doppler channels, and if its value exceeds a certain threshold a signal is considered acquired with a corresponding Doppler velocity v_{det} and signal start t_{det} . The estimated Doppler shift and timing offset are removed and the constituent frequency bands are separately basebanded

$$u_k(t) = D_{-v_{\text{det}}} [u(t - t_{\text{det}})] \exp[-i(\omega_k - \omega_c)t] \quad (6)$$

for $k = 1, \dots, K$. A brick-wall bandpass filter is used to remove energy outside each frequency band

$$x_k(t) = B \int_0^{NT} \text{sinc}(B(t - \tau)) u_k(\tau) d\tau. \quad (7)$$

This filter prevents aliasing when the signal is further downsampled, but does not modify signal and noise within the band. Further filtering is left to the adaptive equalizer of the next section,

which naturally assumes the task of a filter matched to the received signal. An overall rms normalization is finally applied to provide a favorable starting point for the equalization process

$$y_k(t) = x_k(t) \left(\frac{1}{KNT} \sum_{k=1}^K \int_0^{NT} x_k(t) x_k^*(t) dt \right)^{-1/2}. \quad (8)$$

The sole purpose of the normalization is to speed up equalizer convergence by presenting samples whose magnitude is approximately known, which enables an appropriate choice for the initial condition of the adaptive filter.

B. Equalization

The equalizer structure is depicted in the right part of Fig. 2. The baseband signals $y_k(t)$ are downsampled to a samples per symbol, to be phase shifted and to be fed to a fractionally spaced (bT/a) multichannel equalizer with L taps per branch. The phase shifts and equalizers are updated in different consecutive forward and backward passes, indicated by the index $m = 1, 2, \dots, M$. Odd indices are related to forward passes, and even indices are related to backward passes. To obtain the n th symbol estimate $\hat{z}^{(m)}(n)$ in the m th pass, each band is separately phase shifted and equalized, and the results are summed

$$\hat{z}^{(m)}(n) = \sum_{k=1}^K \left(\mathbf{y}_{k,n}^{(m)} \right)^T \mathbf{c}_{k,n\pm 1}^{(m)} \quad (9)$$

where

$$\mathbf{y}_{k,n}^{(m)} = \begin{bmatrix} y_k(nT - (L-1)bT/(2a)) \\ y_k(nT - (L-3)bT/(2a)) \\ \vdots \\ y_k(nT + (L-3)bT/(2a)) \\ y_k(nT + (L-1)bT/(2a)) \end{bmatrix} \exp[-i\theta_k^{(m)}(n \pm 1)]. \quad (10)$$

Here, $\theta_k^{(m)}(n \pm 1)$ is the “previous” phase shift for the k th carrier and the m th sweep, and $\mathbf{c}_{k,n\pm 1}^{(m)}$ is the “previous” equalizer for the k th carrier and the m th sweep. In \pm , $-$ is selected for a forward pass and $+$ for a backward pass, and thus “previous” could imply “past” or “future.” This convention will hold throughout this paper. Notice that the L samples in $\mathbf{y}_{k,n}^{(m)}$ have been selected so as to center the strongest multipath arrival, of

the detector output, in the feedforward filters at the start of the equalization process.

To guide the updates of the phase shifts and equalizers, a reference symbol $z_{\text{ref}}^{(m)}(n)$ is adopted according to four criteria

$$z_{\text{ref}}^{(m)}(n) = \begin{cases} z(n), & n \in Q_{\text{IT}} \vee n \in Q_{\text{PT}} \\ +1, & n \in Q_{\text{TC}} \wedge \gamma_0^{(m-1)}(n) > \Gamma \\ -1, & n \in Q_{\text{TC}} \wedge \gamma_1^{(m-1)}(n) > \Gamma \\ \text{sgn} \{ \Re \{ \hat{z}^{(m)}(n) \} \}, & \text{otherwise} \end{cases} \quad (11)$$

where Q_{IT} denotes the set of initial training symbols, Q_{PT} is the set of periodic training symbols, and Q_{TC} is the set of turbo encoded symbols. $\gamma_0^{(m-1)}(n)$ and $\gamma_1^{(m-1)}(n)$ are the probabilities that the n th bit is equal to 0 or 1, respectively. These probabilities are computed from the posterior log-likelihood ratio (LLR) obtained from the turbo decoder in the $(m-1)$ th pass; see Section III-D. If one of these probabilities exceeds a pre-determined threshold Γ , the corresponding symbol effectively joins in as an additional training symbol. After selection of the reference symbol, a single error signal is computed as

$$\varepsilon^{(m)}(n) = z_{\text{ref}}^{(m)}(n) - \hat{z}^{(m)}(n). \quad (12)$$

LLR thresholding has also been used in [21] and [22], although in these papers, the additional training is employed to estimate frequency-flat fading channels. In our case, it is instrumental in estimating the coefficients of equalizers that can handle frequency-selective fading channels.

C. Adaptive Filtering

To avoid double updates at the signal borders, the forward passes run from $n = 2$ to $n = N$ and the backward passes run from $n = N - 1$ to $n = 1$. Phase estimates and equalizer coefficients are updated as follows. The residual phase offsets $\theta_k^{(m)}(n)$ are all derived from a single phase shift $\theta^{(m)}(n)$ tuned to the overall center frequency ω_c . Carrier recovery is achieved with an integrated digital phase-locked loop (PLL) [2], comparing the phase angle of the equalized symbol $\hat{z}^{(m)}(n)$ with that of the reference symbol $z_{\text{ref}}^{(m)}(n)$

$$\Phi^{(m)}(n) = \arg \left[\left(z_{\text{ref}}^{(m)}(n) \right)^* \hat{z}^{(m)}(n) \right] \quad (13)$$

$$\theta^{(m)}(n) = \theta^{(m)}(n \pm 1) + K_1 \Phi^{(m)}(n) + K_2 \sum_{n'=n_1}^{n_2} \Phi^{(m)}(n') \quad (14)$$

$$\theta_k^{(m)}(n) = \frac{\omega_k}{\omega_c} \theta^{(m)}(n) \quad (15)$$

where $n_1 = 2$ and $n_2 = n$ for the forward passes and $n_1 = n$ and $n_2 = N - 1$ for the backward passes, and where K_1 and K_2 denote the proportional and integral phase-tracking constants. The PLL is initialized with $\theta^{(1)}(1) = 0$, adopting

$$\theta^{(m)}(N) = \theta^{(m-1)}(N) \quad (16)$$

at the boundaries if m is even and

$$\theta^{(m)}(1) = \theta^{(m-1)}(1) \quad (17)$$

if m is odd.

The equalizers $\mathbf{c}_{k,n}^{(m)}$ are updated using a separate RLS scheme for each frequency band, yet guided by the common error signal $\varepsilon^{(m)}(n)$. If $z_{\text{ref}}^{(m)}(n)$ is set according to the first three criteria in (11), the Kalman gain vector $\mathbf{g}_{k,n}^{(m)}$, filter coefficients $\mathbf{c}_{k,n}^{(m)}$, and the inverse correlation matrix $\mathbf{P}_{k,n}^{(m)}$ are updated as

$$\mathbf{g}_{k,n}^{(m)} = \frac{\mathbf{P}_{k,n \pm 1}^{(m)} \left(\mathbf{y}_{k,n}^{(m)} \right)^*}{\lambda + \sum_{k'=1}^K \left(\mathbf{y}_{k',n}^{(m)} \right)^T \mathbf{P}_{k',n \pm 1}^{(m)} \left(\mathbf{y}_{k',n}^{(m)} \right)^*} \quad (18)$$

$$\mathbf{c}_{k,n}^{(m)} = \mathbf{c}_{k,n \pm 1}^{(m)} + \mathbf{g}_{k,n}^{(m)} \varepsilon^{(m)}(n) \quad (19)$$

$$\mathbf{P}_{k,n}^{(m)} = \lambda^{-1} \left[\mathbf{P}_{k,n \pm 1}^{(m)} - \mathbf{g}_{k,n}^{(m)} \left(\mathbf{y}_{k,n}^{(m)} \right)^T \mathbf{P}_{k,n \pm 1}^{(m)} \right] \quad (20)$$

where λ denotes the RLS forgetting factor. Otherwise, the filter coefficients are temporarily frozen

$$\mathbf{g}_{k,n}^{(m)} = \mathbf{g}_{k,n \pm 1}^{(m)} \quad (21)$$

$$\mathbf{c}_{k,n}^{(m)} = \mathbf{c}_{k,n \pm 1}^{(m)} \quad (22)$$

$$\mathbf{P}_{k,n}^{(m)} = \mathbf{P}_{k,n \pm 1}^{(m)}. \quad (23)$$

The update equations (18)–(20) are derived from a single standard RLS update [20], where all frequency bands are combined in a single vector

$$\mathbf{y}_n^{(m)} = \left[\left(\mathbf{y}_{1,n}^{(m)} \right)^T, \dots, \left(\mathbf{y}_{K,n}^{(m)} \right)^T \right]^T \quad (24)$$

by assuming that all cross correlations between frequency bands are negligible. This assumption allows each equalizer branch $\mathbf{c}_{k,n}^{(m)}$ to be updated separately, which reduces the computational complexity of the RLS tap update by a factor K . This comes at no cost in performance, as shown in Section IV. The adaptive filter is initialized with $\mathbf{c}_{k,0}^{(1)} = \mathbf{0}_L$ and $\mathbf{P}_{k,0}^{(1)} = \mathbf{I}_{L \times L}$, which is an appropriate initialization of the inverse correlation matrix considering the normalization (8) of the received signal. At the signal boundaries, the following convention is adopted to switch between forward and backward equalization sweeps: $\mathbf{c}_{k,N}^{(m)} = \mathbf{c}_{k,N}^{(m-1)}$ and $\mathbf{P}_{k,N}^{(m)} = \mathbf{P}_{k,N}^{(m-1)}$ if m is even, and $\mathbf{c}_{k,1}^{(m)} = \mathbf{c}_{k,1}^{(m-1)}$ and $\mathbf{P}_{k,1}^{(m)} = \mathbf{P}_{k,1}^{(m-1)}$ if m is odd. In this manner, the equalizer operates back and forth, improving the bit error ratio (BER) in cases with a slow initial convergence and more generally through an increase of the number of training symbols via (11).

D. Computation of Bit Probabilities

After every forward or backward equalization stage, an LLR is computed for the equalized bits. On the assumption that the symbol scatter in the complex plane is described by Rayleigh distributions, the constellation clouds are described by normal distributions with mean values $\pm \mu^{(m)}$ and variance $(\sigma^{(m)})^2$ after projection on the real axis. A minimum-variance unbiased estimate of $\mu^{(m)}$ is obtained by exploiting knowledge of the periodic training

$$\mu^{(m)} = \frac{1}{N_{\text{PT}}} \sum_{n \in Q_{\text{PT}}} z(n) \Re \left\{ \hat{z}^{(m)}(n) \right\} \quad (25)$$

with a corresponding variance

$$\left(\sigma^{(m)}\right)^2 = \frac{1}{N_{\text{PT}} - 1} \sum_{n \in Q_{\text{PT}}} \left[\Re\left(\hat{z}^{(m)}(n)\right) - \mu^{(m)} z(n) \right]^2. \quad (26)$$

The mean and the variance can be computed for the whole signal, per code block, or just any time span that holds a statistically adequate number of training symbols. As the SNR decreases, the variance $(\sigma^{(m)})^2$ increases and the mean $\mu^{(m)}$ decreases, which is a well-known property of Wiener filters. The prior LLR follows as

$$\begin{aligned} \Lambda_{\text{in}}^{(m)}(n) &= \ln \left(\frac{\exp \left[-\frac{(\Re(\hat{z}^{(m)}(n)) - \mu^{(m)})^2}{2(\sigma^{(m)})^2} \right]}{\exp \left[-\frac{(\Re(\hat{z}^{(m)}(n)) + \mu^{(m)})^2}{2(\sigma^{(m)})^2} \right]} \right) \\ &= \frac{2\mu^{(m)} \Re(\hat{z}^{(m)}(n))}{(\sigma^{(m)})^2}, \quad n \in Q_{\text{TC}}. \end{aligned} \quad (27)$$

A standard turbo decoder is used to decode the encoded bits [19]. As an input it takes the prior LLR $\Lambda_{\text{in}}^{(m)}(n)$, and the output consists of the posterior LLR $\Lambda_{\text{out}}^{(m)}(n)$. Probabilities are computed from the posterior LLR

$$\begin{aligned} \gamma_0^{(m)}(n) &= 1 - \gamma_1^{(m)}(n) \\ &= \frac{\exp(\Lambda_{\text{out}}^{(m)}(n))}{1 + \exp(\Lambda_{\text{out}}^{(m)}(n))}, \quad n \in Q_{\text{TC}} \end{aligned} \quad (28)$$

for bits being zero or one after the m th pass. Output bits are obtained from hard decisions based on these probabilities.

E. Discussion

Unlike the bank of feedforward filters, the PLL is updated uninterruptedly, using unconditional hard decisions if nothing better is available. The reason is that the PLL is less sensitive to incorrect decisions than the equalizer. At low SNR, temporary freezing of the equalizer coefficients improves matters, whereas freezing the phase deteriorates matters. Inclusion of a feedback section would render the equalizer even more sensitive to incorrect decisions. It is technically possible to add a feedback filter to the receiver, updating and freezing its coefficients just like those of the feedforward filters. However, it is inexpedient to stop the symbol feedback itself. Since a feedback section requires an uninterrupted supply of reliable soft or hard decisions, or training, it is not suitable for use at very low SNRs. A feedback filter would also be of limited value for the maximum-phase impulse responses of the channels encountered in Section IV.

As to the iterative equalization, the present strategy differs from the standard turbo equalization approaches [13]–[16]. Those methods rely on a channel estimate and apply in each iteration step an equalizer whose coefficients are based on this estimate and some kind of soft symbol information. This paper proposes an *adaptive* turbo equalization scheme, which bypasses channel estimation and updates the equalizer directly using soft symbol information. The state of the art in adaptive turbo equalization can be found in [13], [17], and [18], but our

method differs from these works in more than one way. First, these papers consider only forward sweeps. In every pass, both a feedforward filter and a feedback filter are adopted, where the latter basically implements interference cancellation using soft/hard symbol decisions obtained from the decoder in the previous pass. The feedforward and feedback filters, of the examples in [13], [17], and [18] that bypass channel estimation, are directly computed via output error minimization, exploiting training symbols and soft/hard symbol decisions (hard symbol decisions obtained before the decoder, or soft/hard symbol decisions obtained after the decoder in the previous pass). The present approach improves upon [17] by working with forward and backward passes, utilizing preadapted filters at the signal boundaries as the initial condition for the next pass. Moreover, instead of using soft or hard symbol decisions to update the filters, the multiband feedforward filters are updated with hard symbol decisions, but only if these symbols are reliable. Filters are not updated for unreliable symbols. For the data described in Section IV, this approach outperforms at least the method that uses unconditional hard-decision updates.

F. Parameters

The number of filter taps is set at $L = 14$, the forgetting factor $\lambda = 0.999$, the phase tracking constants $K_1 = 2 \times 10^{-2}$ and $K_2 = 1 \times 10^{-4}$, the probability threshold $\Gamma = 0.9$, and $a = 4$ and $b = 3$. The equalizer taps are thus fractionally spaced at $3T/4$, which is an appropriate choice for the selected raised-cosine rolloff factor $\beta = 1/3$ [20, pp. 631–635]. Fourteen taps then correspond to a time-delay span of 30.4 ms. Constellation statistics (25) and (26) are computed per code block. All these parameters are fixed for the results presented in Section IV, unless stated otherwise.

Soon after the execution of the sea trial described in Section IV-A, it became evident that the receiver performed better than anticipated. Its performance was limited by failure of detection rather than failure of the equalizer to deliver. Therefore, to find the limits of the adaptive receiver, 128 turbo coded bits are “borrowed” for detection, and detection only. Together with the existing m -sequence of length 127, they make a detection preamble of 255 symbols. Its detection performance is similar to that of a true length-255 m -sequence, which would come at a small decrease in effective data rate. Signal detection is performed with a bank of 101 Doppler replicas running from -4 to $+4$ m/s in 8-cm/s steps.

IV. SEA TRIALS, RESULTS, AND DISCUSSION

A. Sea Trials

Sea trials were conducted in northern Europe, in August 2007. This paper treats experiments in the Baltic Sea, where the MCSS signal was transmitted with a prototype acoustic modem. The area was just northeast of the Danish island Bornholm. At a water depth of 70 m, measured sound-speed profiles (SSPs) reveal a local minimum at a depth of about 40 m. The sound channel thus created acts as an acoustic waveguide, and, together with a relatively low salinity of about 10, allows long-range signaling. Fig. 3 shows the setup. The modem was suspended in the sound channel through the moon pool of a surface ship. This ship was neither sailing nor anchored, but

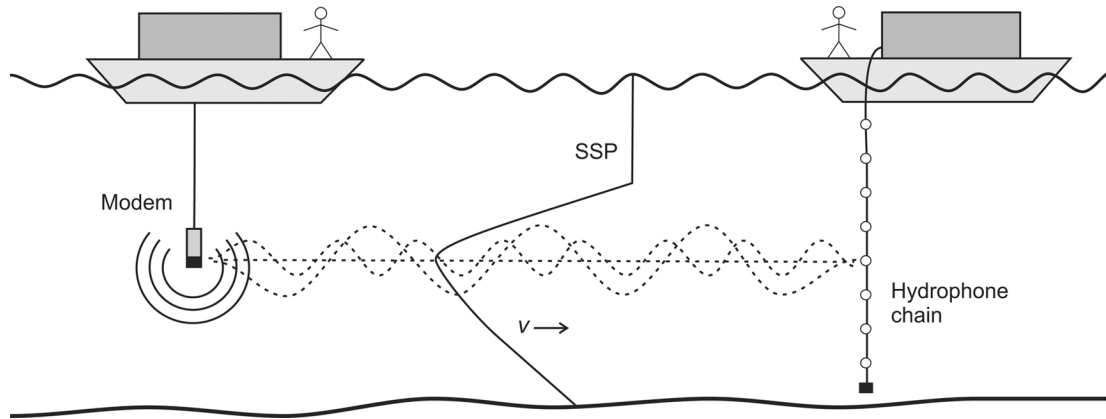


Fig. 3. Depiction of the Baltic sea trial. The figure also sketches the SSP and a few rays trapped in the sound channel.

used dynamic positioning to remain at a given location during communication experiments. An eight-element vertical hydrophone chain was deployed from another, anchored ship. A single element is considered for the analysis, located within the sound channel at a depth of 50 m. The multicarrier modulated signal was part of a periodic broadcast schedule comprising various “covert” modulations and an overt channel probe signal. A cycle with eight different waveforms was repeatedly broadcast, and with each cycle the source level of all except the probe was reduced by 2 dB. Receive SNRs are estimated as explained in [23] and have an uncertainty of about 2 dB.

Impulse responses measured in the Baltic sound channel display a crescendo of multipath arrivals, followed by a decay on a shorter time scale. Power delay profiles for the channels to be analyzed in Sections IV-B and IV-C are shown in Fig. 4. With the transmitter and receiver depths fixed, the range is the chief variable. A dense structure of multipath arrivals is observed, with the delay spread increasing with range. The figure also exhibits characteristic Doppler spectra, which are quite narrow for the first two channels. Indeed, with the nearly stationary surface ships there is little relative transmitter/receiver motion, and modem signals trapped in the sound channel experience no surface interactions. The coherence time of these channels is tens of seconds. The 38-km scenario differs in that the TX ship was towing the source, transferring wave motion onto the transmitter. This motion introduces a time-variable Doppler shift that adds to the Doppler variance. A second reason for the broadening of the Doppler spectrum is the time-variable geometry, i.e., a range which varies with time, which translates as a time-variable impulse response and true Doppler spreading of the channel. The time-variable Doppler shift, a common feature of all multipath arrivals [24], is counterpoised by the integrated PLL. By contrast, the Doppler spreading of the channel itself requires updates of the equalizer coefficients.

B. Data Recorded at Sea

Two sea experiments are analyzed in terms of BER and symbol-scatter statistics. The modem was used to broadcast the MCSS waveform over ranges of 8 and 52 km, at a carrier frequency $f_c = 3.3$ kHz. Fig. 4 shows that the main difference between these fixed-geometry scenarios is a significantly longer delay spread at 52 km. Twenty multicarrier signals

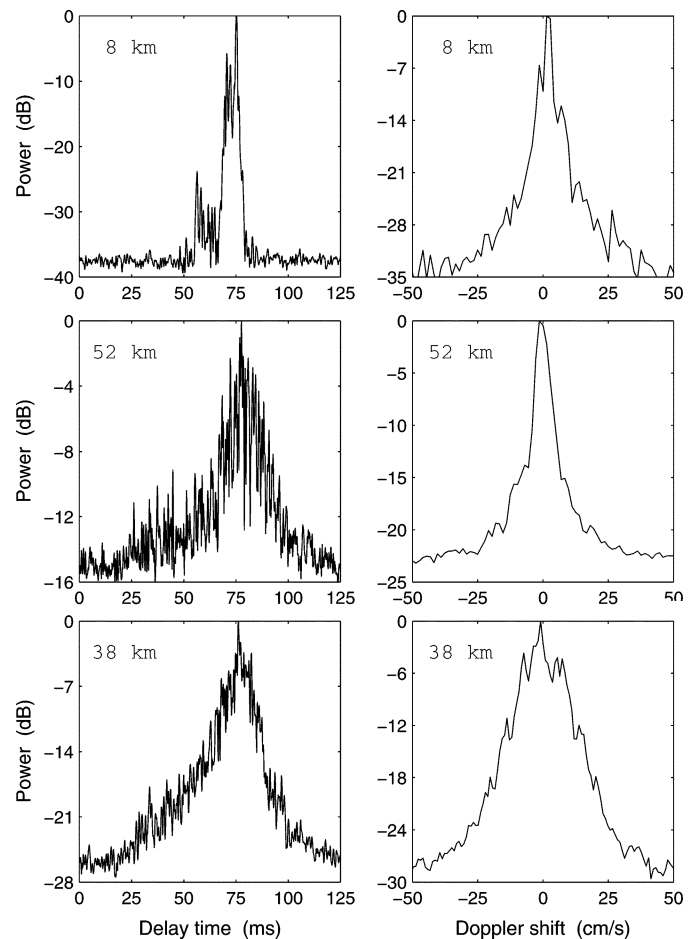


Fig. 4. Power delay profiles and Doppler spectra for channels analyzed using data recorded at sea (8 and 52 km) and a more dynamic scenario mimicked with a channel simulator (38 km). The Doppler spectra are shown after complete removal of the mean Doppler shift; see [24] for a description of the employed probe signal and computation method.

were transmitted over the 8-km range. Table I only lists the last ten, which are in the interesting regime of low SNR. The observed trend of -2 dB per cycle adds to the credibility of the SNR estimates, which also applies to the 52-km results in Table II. Both tables show a gradual increase of the uncoded BER as the SNR decreases. There are irregularities due to the

TABLE I
SIGNALS RECEIVED OVER AN 8-km RANGE: MEAN AND STANDARD DEVIATION, AND NUMBER OF BIT ERRORS BEFORE AND AFTER THE TURBO DECODER

SNR (dB)	μ		σ		uncoded BER $\times 5760$		coded BER $\times 1911$	
	$M = 1$	$M = 3$	$M = 1$	$M = 3$	$M = 1$	$M = 3$	$M = 1$	$M = 3$
+1.1	0.942	0.944	0.175	0.153	0	0	0	0
-0.7	0.943	0.943	0.181	0.161	0	0	0	0
-2.1	0.883	0.880	0.272	0.240	9	2	0	0
-4.9	0.781	0.783	0.344	0.303	92	35	0	0
-6.1	0.858	0.856	0.282	0.251	22	6	0	0
-8.5	0.780	0.787	0.342	0.303	116	40	0	0
-9.2	0.680	0.680	0.398	0.353	236	129	0	0
-12.1	0.461	0.468	0.443	0.369	843	609	0	0
-13.9	0.274	0.288	0.443	0.342	1450	1213	431	260
-16.5	0.248	0.263	0.439	0.342	1649	1379	523	410

TABLE II
SIGNALS RECEIVED OVER A 52-km RANGE: MEAN AND STANDARD DEVIATION, AND NUMBER OF BIT ERRORS BEFORE AND AFTER THE TURBO DECODER. A DASH INDICATES FAILURE OF DETECTION

SNR (dB)	μ		σ		uncoded BER $\times 5760$		coded BER $\times 1911$	
	$M = 1$	$M = 3$	$M = 1$	$M = 3$	$M = 1$	$M = 3$	$M = 1$	$M = 3$
+0.6	0.845	0.872	0.269	0.231	5	1	0	0
-1.9	0.846	0.875	0.279	0.239	12	2	0	0
-4.3	0.663	0.713	0.375	0.328	233	110	0	0
-6.5	0.688	0.706	0.392	0.336	250	106	0	0
-8.5	0.718	0.747	0.373	0.322	178	61	0	0
-9.2	0.514	0.535	0.438	0.369	706	434	0	0
-12.7	0.473	0.493	0.429	0.374	845	554	0	0
-14.4	0.324	0.349	0.448	0.361	1353	965	358	0
-17.6	—	—	—	—	—	—	—	—
-19.2	—	—	—	—	—	—	—	—

time-varying nature of both signal and noise, but trends are clear. Although the receiver computes statistics per code block, the mean μ and standard deviation σ are here averaged over all N_{PT} training symbols for convenience of presentation. As the SNR decreases, the constellation clouds shift toward the origin and grow larger. The iteration gain is evident from the difference between the $M = 1$ and $M = 3$ columns. Successive equalization stages reduce the standard deviation and BER. At low SNRs, the iterations also increase the value of μ a little, which contributes to the BER reduction. Section IV-C provides a more detailed examination of the influence of adaptive turbo equalization on the BER.

The rate 1/3 turbo code is capable of handling up to 15%–20% of bit errors, depending on the fidelity of the prior LLR (27). Tables I and II show that the receiver correctly delivers the user message at SNRs down to -12 and -14 dB, respectively. This is perhaps surprising as the latter figure corresponds to the “more difficult” impulse response, but it

is within the ≈ 2 -dB uncertainty in the SNR estimates. At least the receiver does not seem to be hindered by the longer delay spread. At high SNR, at comparable values of the input SNR, there are more uncoded bit errors for the 52-km channel than at 8 km. This difference seems to disappear at very low SNR, where the contribution of multipath to the total signal-to-interference-plus-noise ratio becomes less important. The communication link ceases to exist, owing to failure of detection, for the ninth and tenth received signal at 52 km.

Fig. 5 illustrates the receiver operation for the sixth signal of Table II, received at an SNR of about -10 dB, after a single equalization pass. The top-left panel shows the correlator output for a 10-s interval, including detection at 6 s. The power spectral density in the top-right panel is averaged over the duration of the signal and just bears evidence of a few frequency bands between 3 and 5 kHz. At lower frequencies, the signal energy is overpowered by the colored noise. The MSE $E(|\varepsilon^{(1)}(n)|^2)$, averaged over 100 symbols, and the phase estimate $\theta^{(1)}(n)$ are shown

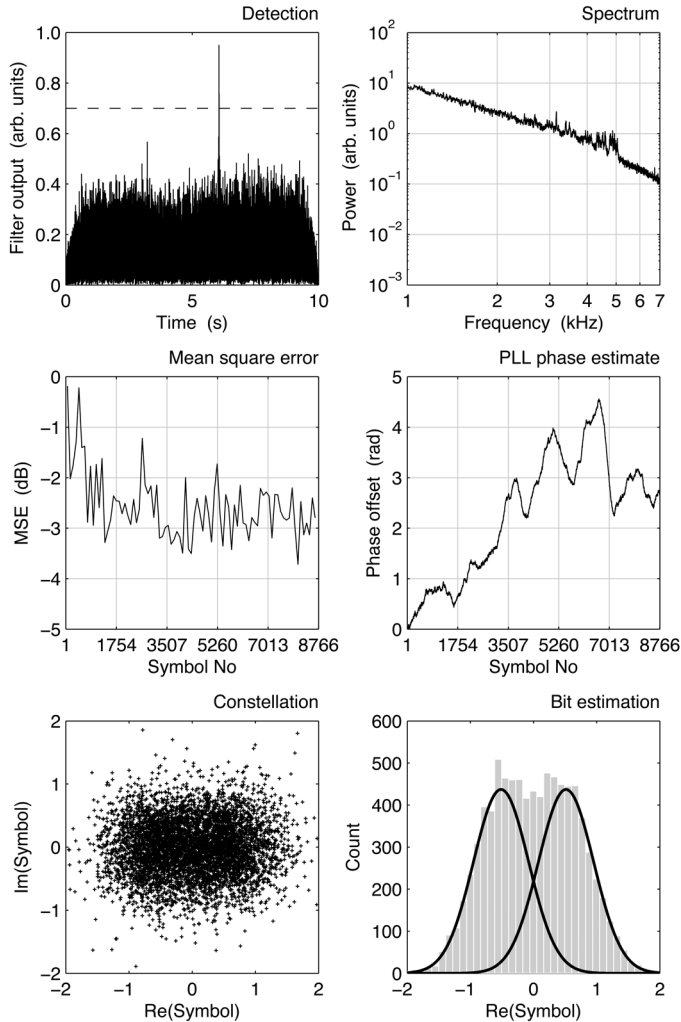


Fig. 5. Receiver diagnostics for an example reception over 52 km, an estimated SNR of ≈ -10 dB, and a single equalization sweep. For convenience of plotting, the histogram and curves in the bit estimation panel are here computed for the entire signal.

in the middle panels. The bottom panels display the equalized symbols $\hat{z}^{(1)}(n)$, excluding the initial training, and a histogram of their real parts. Thick black curves represent the normal distributions found in the numerator and the denominator of (27). The shape of these curves is obtained from the periodic training, and their amplitude is simply scaled to obtain the same total area under curves and bars.

The situation for $M = 3$ is shown in Fig. 6, which omits the unaltered detection and spectrum panels. An overall improvement is noticed for the MSE, notably during the first thousand or so symbols, as the equalizer has already adapted to the channel when it commences the final forward pass. However, since the MSE is computed relative to the theoretical constellation points with unity magnitude, it is of limited significance as a quality measure for equalized symbols which congregate much closer to the origin. The residual phase is nearly identical to that of the first pass, which suggests that the iteration gain is mostly achieved by better adaptation of the equalizer coefficients. Finally, the constellation clouds are better separated, although this

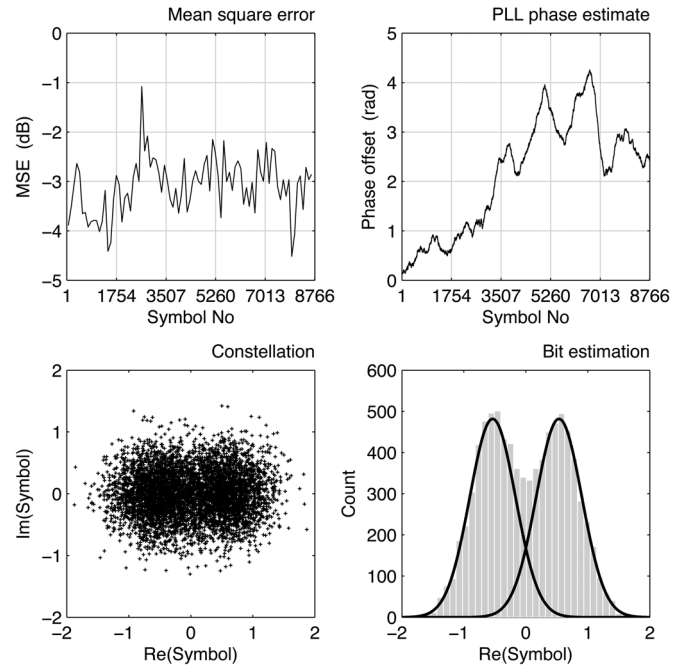


Fig. 6. Bottom four panels of Fig. 5, but after three equalization sweeps.

is easier to tell from the histogram than from the clouds themselves. The bars and curves in Figs. 5 and 6 further reveal an excellent match, inspiring confidence in the application of a normal distribution to compute the prior LLR.

C. Synthetic Data

To investigate the importance of various receiver elements, the waveform is passed through a filter channel. The simulation method is the replay mode of the channel simulator described in [24], using the same channel that was examined and validated in that paper. It concerns a fully realistic channel archived during the same sea experiments on the Baltic Sea. A difference with the relatively static channels of Section IV-B is that a towed source was used, operated at a carrier frequency $f_c = 5$ kHz and towed at a nominal speed of 2.5 m/s. The bottom panels of Fig. 4 give the power delay profile and Doppler spectrum for this scenario, which corresponds to a range of 38 km. The channel covers a delay-time interval of 100 ms and has a coherence time of 5 s [24]. The filtered signal is further characterized by a time-variable Doppler shift caused by motion of the tow ship on the waves. It is complemented with sea noise scaled to achieve a given SNR, which is exact in the time-frequency window occupied by the signal. Since a single channel realization and a single noise recording are used in Figs. 7 and 8, and since the total number of bits is relatively small, the resulting BER statistics are not overwhelming. Nonetheless, the results illustrate the differences between the various approaches well enough qualitatively, and allow a quantitative comparison for this specific channel. The BER is shown for an uncoded rate of 225 b/s, whereas the transition between a nonzero and zero coded BER at 75 b/s is indicated on the horizontal axes. Proper detection and synchronization is enforced for all shown curves. This does not affect the critical SNR for the coded BER, but it

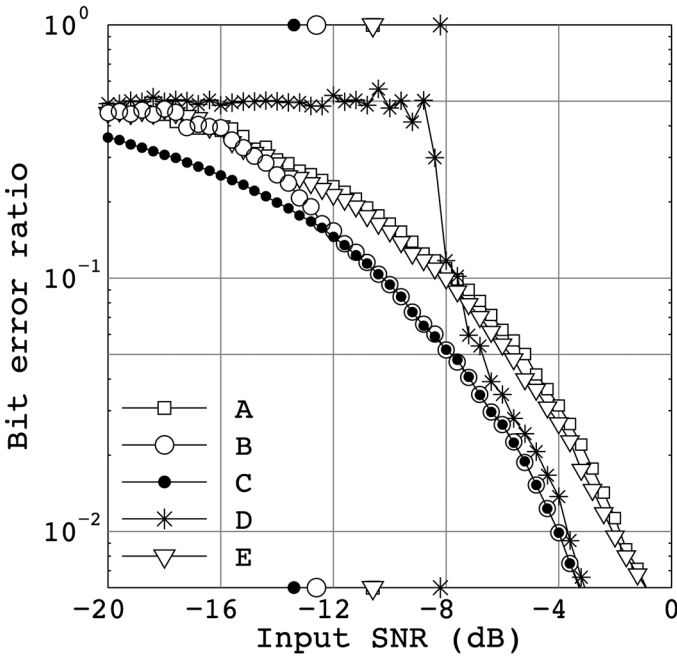


Fig. 7. Uncoded BER for the replay channel. (A) Proposed receiver with $M = 1$. (B) Proposed receiver with $M = 3$. (C) Equalizer in full training mode ($M = 3$). (D) Equalizer in decision-directed mode after initial training ($M = 3$). (E) Taps updated only during training ($M = 3$). The critical SNR for the coded BER is indicated on the horizontal axes.

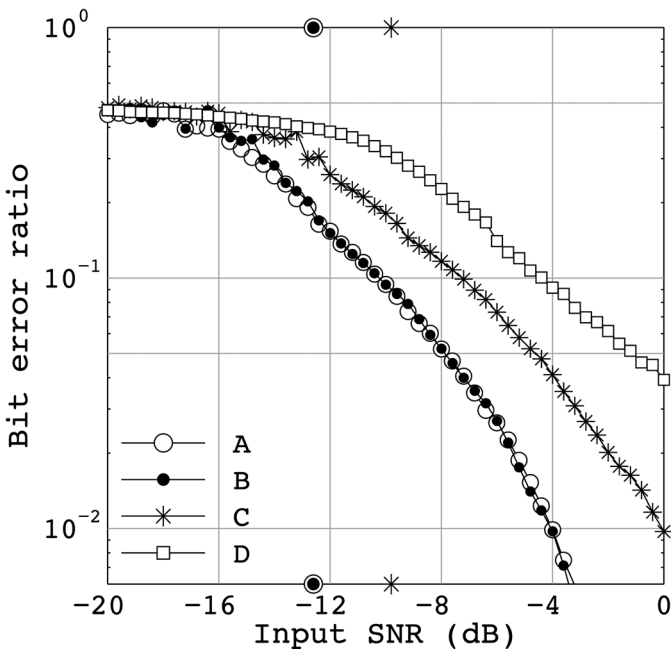


Fig. 8. Uncoded BER for the replay channel. (A) Proposed receiver. (B) Joint multiband RLS update. (C) $K = 4$ using bands 1, 3, 5, and 7. (D) PLL switched off. $M = 3$ for all cases. The critical SNR for the coded BER is indicated on the horizontal axes, is the same for A and B, and amounts to +2 dB for D.

allows the uncoded BER curves to continue smoothly toward -20 dB. Detection otherwise fails at -14 dB.

Fig. 7 shows the BER curves after $M = 1$ (curve A) and $M = 3$ (curve B) equalizer stages. For $M = 1$, the tap coefficients are updated only during the initial and periodic training periods. $M = 2$ (not shown) equalizes in reverse and improves

upon the $M = 1$ performance by assigning bits, which received a probability $> \Gamma$ of being correct at the end of the first stage, as new training symbols. $M = 3$ starts where $M = 2$ ended, thus has a better starting condition than $M = 1$, and further benefits from the posterior LLR computed at the end of the second stage. More than two iterations (not shown) only yield a marginal further improvement of one or two tenths of a decibel. The figure also includes a reference curve C, obtained by operating the equalizer in training mode throughout the entire signal. That is to say, there is perfect symbol feedback using N training symbols. It is seen that curve B gradually switches between the trajectories of A and C. As the SNR increases, more bits are added as training symbols and B approaches the 100% training curve. Inspection of $\gamma_0^{(2)}(n)$ and $\gamma_1^{(2)}(n)$ reveals that the equalizer is effectively in full training mode at SNRs of -12 dB and higher.

The importance of periodic training at low SNR is illustrated by curves D and E. The former is obtained by using only the first N_{IT} bits for training. Otherwise the equalizer is operated in a routine decision-directed mode, i.e., the periodic training symbols are treated as unknown data symbols and hard decisions are used throughout to compute the error signal. E is obtained by updating the equalizer coefficients only during the designated training periods. The difference with B is a probability threshold $\Gamma = 1$ instead of $\Gamma = 0.9$, which just results in no tap updates for the coded bits. E improves a little upon A because it uses three equalization sweeps instead of one.

At high SNR, D approaches B as more decisions become correct. However, as the SNR decreases D gradually departs from B, and quickly rises to a 50% BER at -8 dB. An increasing number of incorrect decisions results in equalizer divergence. The use of more initial training symbols (not shown) does not help; the underperformance of curve D is due to tracking failure after initial convergence. Curve E shows that it is better to use periodic training, and not update the filter coefficients in between. This does not hold at high SNR, where D outperforms E owing to more numerous tap updates. D has a better channel tracking capability so long as the decisions are mostly correct. Periodic training thus improves the performance at low SNR, but the proposed receiver B shows that it is better still to use periodic training, and, in addition, irregular in-between training when the probability of picking the correct reference symbol is high. A zero coded BER is achieved down to -12.4 dB.

Miscellaneous effects are examined in Fig. 8. Curve A is the same as curve B in Fig. 8 and serves as a reference for the other curves, all of which differ from A in only one respect. B is obtained by switching from K RLS updates with a joint error to a single vector $\mathbf{y}_n^{(m)}$ with length KL . The joint update is initiated with $\mathbf{P}_1^{(1)} = \mathbf{I}_{KL \times KL}$ and $\mathbf{c}_1^{(1)} = \mathbf{0}_{KL}$, where the subscript k is now dropped. Everything else is equal. Although this is the prevalent multichannel RLS approach, there appears to be no advantage of B over A, as the two curves are virtually identical. Justification for approach A is furnished by the low-frequency coherence induced by multipath propagation. The coherence bandwidth is of order T_{delay}^{-1} , where T_{delay} is some characteristic delay spread of the channel. The delay spreads of Fig. 4 easily lead to a frequency coherence much smaller than the sub-band separation of 460 Hz. As a result, the frequency channels

are mutually uncorrelated, and there is no need for a joint RLS update which allows for cross correlations between channels. In the presence of a long delay spread and time variability, the use of separate equalizers may be advantageous even when the channels are correlated. In this case, the separate equalizers offer faster channel tracking, and may outperform the single, long equalizer which does not converge fast enough to operate at the MSE that it would achieve for a static channel.

Since the complexity of the RLS tap update is $\mathcal{O}(KL^2)$ for method A and $\mathcal{O}(K^2L^2)$ for method B, A thus offers a reduced complexity at no cost in performance. In comparison with a single-carrier DSSS receiver which equalizes the chips and covers the same multipath delay span, the computational advantage is even a factor K^2 . One factor of K is then due to the complexity of the RLS tap update itself, and another factor of K is due to the number of tap updates. Although the total receive time also includes operations such as basebanding, which are more demanding for MCSS than for DSSS, the RLS tap update completely dominates the receiver complexity for long delay spreads.

Curve C in Fig. 8 is obtained by feeding four ($k \in \{1, 3, 5, 7\}$) instead of $K = 8$ bands to the multiband equalizer. The performance drops and illustrates the main point of this paper, namely, that the receiver can exploit the diversity created by transmitting the same symbols in parallel frequency bands.

The difference between A and D is the absence of a PLL for the latter, i.e., $K_2 = K_1 = 0$. Although the estimated mean Doppler shift has been removed before equalization, the PLL is still badly needed to track residual phase drifts. A digital PLL integrated in equalizer structures is certainly not new, but its importance cannot be stressed enough. In the absence of a phase-tracking loop, the residual Doppler causes a tap rotation which is difficult for the equalizer to manage. The equalized symbols do not obey Rayleigh statistics, the computed LLR (27) is in error, and the critical coded SNR is off the chart at +2 dB.

Finally, it is remarked that the threshold Γ is not a critical parameter. Its value was kept fixed at 0.9 for all presented results, but a virtually identical performance is obtained with values in the range 0.7–0.95. Outside this region the receiver performance drops, notably for the cases $\Gamma = 0.5$, i.e., hard decisions on the posterior LLR for all turbo coded bits, and $\Gamma = 1$, i.e., no tap updates whatsoever for the coded bits.

V. CONCLUDING REMARKS

An unorthodox modulation scheme is presented to establish reliable acoustic communication in time-varying channels and at low SNR. The main ingredient is joint equalization and de-spreading of parallel frequency bands carrying identical symbol streams. Periodic training and channel coding allow a further reduction of the working SNR. An adaptive turbo equalization scheme is applied, which utilizes the posterior LLR of a previous equalizer pass to selectively add training symbols to a new pass. Ignoring cross correlations between frequency bands, a reduced-complexity RLS channel tracking algorithm is applied without noticeable performance degradation.

Robust operation is demonstrated at SNRs down to -12 dB with an automated receiver and fixed parameters, for an array of

channels with different degrees of delay and Doppler spreading. In terms of SNR per bit, this corresponds to $E_b/N_0 = -12$ dB $-10 \times \log_{10}(R/(KB)) = +5$ dB, with $R = 75$ b/s the net data rate and $KB = 3680$ Hz the total bandwidth. In another paper [23], the proposed communication scheme is compared directly with other “covert” modulations, viz., DSSS [7] and OFDM [12]. Waveforms of these modulations were transmitted during the same experiments, in the same frequency band, and at the same effective data rate as MCSS. With the current implementations of the various receivers, the comparison is in favor of the multiband turbo equalization scheme, especially at long delay spreads, such as the 52-km scenario of Fig. 4, where MCSS delivers at considerably lower SNRs (6–8 dB) than the competition.

If there is need for communication at still lower SNRs, more subbands can be employed to deliver a higher spreading gain at a reduced data rate. Disadvantages of this solution are a reduced channel tracking rate, because the symbol rate is inversely proportional to the number of bands for a given total bandwidth, and an increase of the crest factor. A hybrid form of MCSS and DSSS can also be considered [10], [11]. Temporal diversity in the form of repetition coding, and spatial diversity obtained by application of a hydrophone array, are other options. Together, they yield the prospect of an $I \times J \times K$ equalizer jointly operating on I hydrophones, J repetitions in time, and K frequency bands. At any rate, as the working SNR decreases special attention should also be paid to acquisition, which manifested itself as the Achilles’ heel of a 4-b/s OFDM link [12].

ACKNOWLEDGMENT

The authors would like to thank the entire consortium and management group of the UUV Covert Acoustic Communications project for valuable contributions and a fruitful cooperation.

REFERENCES

- [1] A. J. Paulraj and C. B. Papadias, “Space-time processing for wireless communications,” *IEEE Signal Process. Mag.*, vol. 14, no. 6, pp. 49–83, Nov. 1997.
- [2] M. Stojanovic, J. Catipovic, and J. G. Proakis, “Adaptive multichannel combining and equalization for underwater acoustic communications,” *J. Acoust. Soc. Amer.*, vol. 94, no. 3, pp. 1621–1631, Sep. 1993.
- [3] Q. Wen and J. A. Ritcey, “Spatial diversity equalization applied to underwater communications,” *IEEE J. Ocean. Eng.*, vol. 19, no. 2, pp. 227–241, Apr. 1994.
- [4] M. Stojanovic, J. A. Catipovic, and J. G. Proakis, “Reduced-complexity spatial and temporal processing of underwater acoustic communication signals,” *J. Acoust. Soc. Amer.*, vol. 98, no. 2, pp. 961–972, Aug. 1995.
- [5] T. C. Yang, “A study of spatial processing gain in underwater acoustic communications,” *IEEE J. Ocean. Eng.*, vol. 32, no. 3, pp. 689–709, Jul. 2007.
- [6] L. Freitag, M. Stojanovic, S. Singh, and M. Johnson, “Analysis of channel effects on direct-sequence and frequency-hopped spread-spectrum acoustic communication,” *IEEE J. Ocean. Eng.*, vol. 26, no. 4, pp. 586–593, Oct. 2001.
- [7] E. Sangfelt, B. Nilsson, and J. Israelsson, “Covert underwater communication experiments using DSSS and turbo equalization,” in *Proc. Undersea Defence Technol. Eur.*, Glasgow, U.K., Jun. 2008, paper 11C2.
- [8] N. Yee, J. P. Linnartz, and G. Fettweis, “Multi-carrier CDMA in indoor wireless radio,” in *Proc. IEEE Personal Indoor Mobile Radio Commun. Symp.*, Yokohama, Japan, Sep. 1993, pp. 109–113.
- [9] K. Frazel and L. Papke, “On the performance of convolutionally-coded CDMA/OFDM for mobile communication system,” in *Proc. IEEE Personal Indoor Mobile Radio Commun. Symp.*, Yokohama, Japan, Sep. 1993, pp. 468–472.

- [10] S. Kondo and L. B. Milstein, "Performance of multicarrier DS CDMA systems," *IEEE Trans. Commun.*, vol. 44, no. 2, pp. 238–246, Feb. 1996.
- [11] E. A. Sourour and M. Nakagawa, "Performance of orthogonal multicarrier CDMA in a multipath fading channel," *IEEE Trans. Commun.*, vol. 44, no. 3, pp. 356–367, Mar. 1996.
- [12] G. Leus and P. A. van Walree, "Multiband OFDM for covert acoustic communications," *IEEE J. Sel. Areas Commun.*, vol. 26, no. 9, pp. 1662–1673, Dec. 2008.
- [13] S. Roy, T. M. Duman, V. McDonald, and J. G. Proakis, "High-rate communication for underwater acoustic channels using multiple transmitters and space-time coding: Receiver structures and experimental results," *IEEE J. Ocean. Eng.*, vol. 32, no. 3, pp. 663–688, Jul. 2007.
- [14] R. Koetter, A. C. Singer, and M. Tüchler, "Turbo equalization," *IEEE Signal Process. Mag.*, vol. 21, no. 1, pp. 67–80, Jan. 2004.
- [15] J. F. Sifferlen, H. C. Song, W. S. Hodgkiss, W. A. Kuperman, and J. M. Stevenson, "An iterative equalization and decoding approach for underwater acoustic communication," *IEEE J. Ocean. Eng.*, vol. 33, no. 2, pp. 182–197, Apr. 2008.
- [16] R. Otnes and T. H. Eggen, "Underwater acoustic communications: Long-term test of turbo equalization in shallow water," *IEEE J. Ocean. Eng.*, vol. 33, no. 3, pp. 321–334, Jul. 2008.
- [17] C. Laot, A. Glavieux, and J. Labat, "Turbo equalization: adaptive equalization and channel decoding jointly optimized," *IEEE J. Sel. Areas Commun.*, vol. 19, no. 9, pp. 1744–1752, Sep. 2001.
- [18] Y. Sun, V. Tripathi, and M. Honig, "Adaptive turbo reduced-rank equalization for MIMO channels," *IEEE Trans. Wireless Commun.*, vol. 4, no. 6, pp. 2789–2800, Nov. 2005.
- [19] C. Heegard and S. B. Wicker, *Turbo Coding*. New York: Springer-Verlag, 1998.
- [20] J. G. Proakis, *Digital Communications*, 4th ed. New York: McGraw-Hill, 2001.
- [21] Y. Xu, H.-J. Su, and E. Geraniotis, "Pilot symbol assisted QAM with iterative filtering and turbo decoding over Rayleigh flat-fading channels," in *Proc. IEEE Mil. Commun. Conf.*, Atlantic City, NJ, Oct./Nov. 1999, vol. 1, pp. 86–91.
- [22] H. Niu and J. A. Ritcey, "Iterative channel estimation and decoding of pilot symbol assisted LDPC coded QAM over flat fading channels," in *Proc. 36th Asilomar Conf. Signals Syst. Comput.*, Pacific Grove, CA, Nov. 2002, vol. 2, pp. 2265–2269.
- [23] P. A. van Walree, E. Sangfelt, and G. Leus, "Multicarrier spread spectrum for covert acoustic communications," in *Proc. OCEANS Conf.*, Quebec City, QC, Canada, Sep. 2008, DOI: 10.1109/OCEANS.2008.5151841.
- [24] P. A. van Walree, T. Jenserud, and M. Smedsrud, "A discrete-time channel simulator driven by measured scattering functions," *IEEE J. Sel. Areas Commun.*, vol. 26, no. 9, pp. 1628–1637, Dec. 2008.



Paul van Walree (M'08) received the M.Sc. and Ph.D. degrees in solid-state physics from Utrecht University, Utrecht, The Netherlands, in 1992 and 1997, respectively.

From 1998 to 2009, he was an Underwater Acoustician at the Sonar Department, The Netherlands Organisation for Applied Scientific Research (TNO), The Netherlands. In 2009, he started as a Scientist with the Maritime Systems Department, Norwegian Defence Research Establishment (FFI), Horten, Norway. His research interests include digital underwater communications, channel characterization and simulation, and acoustic signal processing.



Geert Leus (M'01–SM'05) was born in Leuven, Belgium, in 1973. He received the electrical engineering degree and the Ph.D. degree in applied sciences from the Katholieke Universiteit Leuven, Belgium, in June 1996 and May 2000, respectively.

He has been a Research Assistant and a Postdoctoral Fellow of the Fund for Scientific Research, Flanders, Belgium, from October 1996 until September 2003. During that period, he was affiliated with the Electrical Engineering Department, Katholieke Universiteit Leuven. Currently, he is an Associate Professor at the Faculty of Electrical Engineering, Mathematics and Computer Science, Delft University of Technology, Delft, The Netherlands. During summer 1998, he visited Stanford University, and from March 2001 until May 2002, he was a Visiting Researcher and Lecturer at the University of Minnesota. His research interests are in the area of signal processing for communications.

Dr. Leus received the 2002 IEEE Signal Processing Society Young Author Best Paper Award and the 2005 IEEE Signal Processing Society Best Paper Award. He is the Chair of the IEEE Signal Processing for Communications Technical Committee, and an Associate Editor for the IEEE TRANSACTIONS ON SIGNAL PROCESSING and the *EURASIP Journal on Applied Signal Processing*. In the past, he has served on the Editorial Board of the IEEE SIGNAL PROCESSING LETTERS and the IEEE TRANSACTIONS ON WIRELESS COMMUNICATIONS.